Rough-wall channel analysis using suboptimal control theory

By O. Flores†, J. Jiménez ‡ AND J. Templeton

1. Introduction

The original aim of this work was to shed some light on the physics of turbulence over rough walls using large-eddy simulations and the suboptimal-control wall boundary conditions introduced by Nicoud *et al.* (2001). It was hoped that, if that algorithm was used to fit the mean velocity profile of the simulations to that of a rough-walled channel, instead of to a smooth one, the wall stresses introduced by the control algorithm would give some indication of what aspects of rough walls are most responsible for the modification of the flow in real turbulence. It was similarly expected that the structure of the resulting velocity fluctuations would share some of the characteristics of rough-walled flows, thus again suggesting what is intrinsic and what is accidental in the effect of geometric wall roughness.

A secondary goal was to study the effect of 'unphysical' boundary conditions on the outside flow by observing how a relatively major change of the target velocity profile, and therefore presumably of the applied wall stresses, modifies properties such as the dominant length scales of the velocity fluctuations away from the wall.

As will be seen below, this secondary goal grew more important during the course of the study, which was carried out during a short summer visit of the first two authors to the CTR. It became clear that there are open questions about the way in which the control algorithm models the boundary conditions, even for smooth walls, and that these questions make the physical interpretation of the results difficult. Considerable more work in that area seems to be needed before even relatively advanced large-eddy simulations, such as these, can be used to draw conclusions about the physics of wall-bounded turbulent flows.

The numerical method is the same as in Nicoud *et al.* (2001). The modifications introduced in the original code are briefly described in §2, but the original paper should be consulted for a full description of the algorithm. The results are presented in §3 and summarized in §4. The elementary properties of turbulence over rough walls which are used in the text have been taken from recent reviews such as Raupach *et al.* (1991) or Jiménez (to appear in 2004).

2. Simulations

Turbulent channel flow has been simulated using the code presented by Nicoud *et al.* (2001) with $Re_\tau = u_\tau h/\nu = 1000$, where u_τ is the friction velocity and h is the channel half-width. The coordinates used are x, y and z, indicating streamwise, wall-normal and spanwise directions. The streamwise and spanwise periodicity lengths are $L_x = 2\pi$ and $L_z = 2\pi/3$ for all the cases presented here. Except when explicitly noted to the contrary,

† School of Aeronautics, Universidad Politécnica, 28040 Madrid, Spain
‡ Also School of Aeronautics, Universidad Politécnica, 28040 Madrid, Spain

	Re_τ	Δx^+	Δy^+	Δz^+	L_x/h	L_z/h	$N_x \times N_y \times N_z$	α^+	ΔU^+
S1	1000	196	61	65	2π	$2\pi/3$	$32 \times 33 \times 32$	6×10^{-2}	0
S2	1000	196	61	65	2π	$2\pi/3$	$32 \times 33 \times 32$	1.5×10^{-2}	0
R1	1000	196	61	65	2π	$2\pi/3$	$32 \times 33 \times 32$	6×10^{-2}	9

TABLE 1. Test cases. The subindices x, y and z indicate the streamwise, wall-normal and spanwise directions. The N's are the number of grid points in each direction, the Δ's are the corresponding grid spaces and the L's are box lengths. ΔU^+ is the roughness function, defined in (3.7), and α^+ is the parameter in equation (2.1).

all the variables are normalized with u_τ and h. The superindex $^+$ is used for variables expressed in wall units.

The characteristics of the three main simulations used in this paper are summarized in table 1. The letter **S** indicates smooth channels, and **R** is used for rough ones. The reference velocity profile used for **S1** and **S2** is obtained from a direct simulation by del Álamo *et al.* (2003) with $Re_\tau = 950$. The rough-wall profile is described in the next section.

The LES code uses a standard dynamic Smagorinsky subgrid-scale stress model without explicit grid filtering. The spatial discretization is a second-order finite-difference scheme on a staggered grid, and the time integration is third-order Runge-Kutta with an implicit scheme for the wall-normal viscous terms. The flow is driven by a constant mean pressure gradient that balances the wall stresses, $\overline{\partial_x p}^{\,+} = -1$. The overbar stands for averaging over wall-parallel planes, while $\langle\,\rangle$ will be reserved for temporal averaging. With the single exception described at the end of §3.1, the time step Δt is constant.

The boundary conditions in the streamwise and spanwise directions are periodic, and the impermeability condition is imposed at the walls. The two other boundary conditions are the total shear stresses τ_{xy} and τ_{zy} at each point of each wall. They are adjusted at each time step to minimize a cost function $\mathcal{J}$, which measures the difference between the plane-averaged velocity and a given mean velocity profile U_{ref}.

$$\mathcal{J}(\phi_u, \phi_w) = \int_0^{2h} \left[(\overline{u} - U_{ref})^2 + \overline{w}^2\right] dy + \alpha \left(\overline{\phi_u'^2} + \overline{\phi_w'^2}\right), \tag{2.1}$$

where the control variables are vectors of size $2 \times N_x \times N_z$

$$\phi_u = (\tau_{xy}^w\,|_{y=2h}, -\tau_{xy}^w\,|_{y=0}), \qquad \phi_w = (\tau_{zy}^w\,|_{y=2h}, -\tau_{zy}^w\,|_{y=0}), \tag{2.2}$$

and α is a parameter with dimensions $[\alpha] = L/U^2$ that will be discussed in the next section. Primed variables refer to fluctuations with respect to the plane average, so that $\phi' = \phi - \overline{\phi}$. Note that the global conservation of momentum ensures that $\overline{\phi}$ satisfies

$$\langle\overline{\tau_{xy}^w}\rangle\,|_{y=2h} - \langle\overline{\tau_{xy}^w}\rangle\,|_{y=0} = 1, \tag{2.3}$$

and

$$\langle\overline{\tau_{zy}^w}\rangle\,|_{y=2h} - \langle\overline{\tau_{zy}^w}\rangle\,|_{y=0} = 0, \tag{2.4}$$

but that the instantaneous mean stresses at each wall may oscillate in time.

The minimization of $\mathcal{J}$ implies an iterative scheme in which an adjoint problem is solved in order to compute an estimation for the gradient of the cost function. The

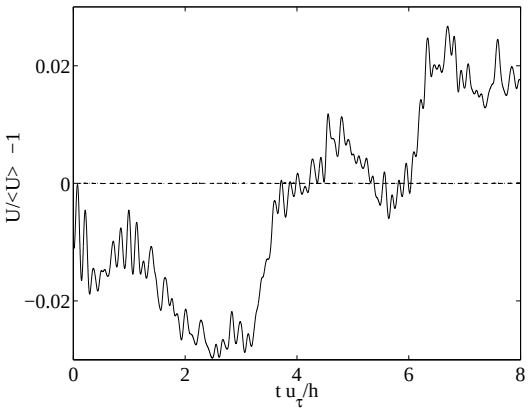

FIGURE 1. Convergence history of the mean velocity at the first plane off the wall, for a smooth-walled channel. ——— , Using the correction (2.5); - - - - , without the correction.

algorithm is suboptimal in the sense that, instead of minimizing the averaged value of $\mathcal{J}$ over a long period of time, the optimization is computed over each individual time step.

Several modifications were introduced in the code during preliminary attempts to match smooth-wall velocity profiles at different Reynolds numbers. The most important was probably the use of the more efficient Brent's method for the optimization scheme (Press *et al.* 1993), instead of the simpler relaxation used by Nicoud *et al.* (2001). This allowed the stable utilization of the algorithm over a wider range of parameters.

Another modification involves the recalculation of the mean wall stress. In the original code, the value of $\overline{\tau_{xy}^w}^{\,+} = u_*^{+2}$ was adjusted at each time step so that the mean velocity in the first plane off the wall satisfied the desired logarithmic law,

$$\frac{\overline{u_{j=1}^+}}{u_*^+} - \frac{1}{\kappa}\log(y_{j=1}^+ u_*^+) - A = 0. \tag{2.5}$$

The idea was that the mean stress is directly determined by the averaged momentum balance, and does not have to be controlled. In each time step the optimum wall stresses were computed using the control algorithm, and their mean value was later corrected to the u_*^2 obtained from (2.5). Notice that $u_*^+ = 1$ satisfies (2.5) whenever $u_{j=1}^+$ is given by the desired logarithmic law. While the general argument is sound in a timed-averaged sense, this procedure 'second-guesses' the control algorithm, since the integrated momentum equation is already incorporated in the code, and its effect was found to be pernicious. The convergence of the original code was oscillatory and the time history of most variables suggested a poorly-damped instability of the control algorithm. Removing the correction step suppressed the oscillations and the instability. Two typical convergence histories, with and without the stress correction, are shown in figure 1. All the results below are obtained without using (2.5).

3. Results

3.1. *The cost function*

A point that needs some discussion is the form of the cost function (2.1). The second term on the right-hand side of (2.1) represents the energy of the control variables ϕ_u and

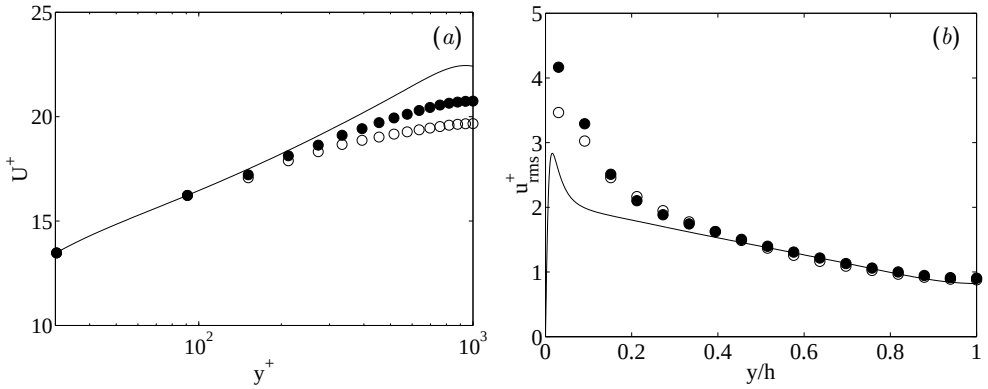

FIGURE 2. Profiles of (a) the mean velocities and (b) the streamwise velocity fluctuations for a smooth-walled channel at $Re_\tau \approx 1000$, using different cost functions. ∘ , case **S1**; • , case **S2**; ——— , direct simulation (del Álamo *et al.*2003).

ϕ_w, and is introduced to ensure numerical stability. The proportionality coefficient α is essentially arbitrary from a physical point of view.

The value of α used here for the cases **S1** and **R1** is the one given by Nicoud *et al.* (2001) as being the smallest one that kept their simulation stable. The effect of a larger α should be to lower the variance of τ^w, weakening the strength of the control, and therefore presumably degrading the quality of the resulting mean profile. It is nevertheless possible to 'overcontrol' a system, in the sense that some properties which are not taken into account in the cost function may be contaminated by the control itself. It was noted by Nicoud *et al.* (2001) that the velocity fluctuations in the simulated channels are stronger than those in direct simulations or in experiments, especially near the wall. Since those fluctuations are driven by the wall stresses, which are in turn influenced by α, it is conceivable that the reason for the high fluctuations is that α was chosen too small.

A measure of the strength of the control is the temporal variability of $\overline{u}$, compared with its 'expected' variation. If the velocities are considered to be uncorrelated random variables, which is probably not too far from the truth for a coarse LES, the expected variance of $\overline{u}$ would be

$$\sigma_P^2 = (N_x N_z)^{-1} \overline{u'^2}, \tag{3.1}$$

which has to be compared with the actual measured value

$$\sigma^2 = \langle (\overline{u} - \langle \overline{u} \rangle)^2 \rangle. \tag{3.2}$$

The ratio σ/σ_P should be of order unity in a natural flow, and its deviation from unity is a measure of the strength of the control.

It is not clear which is the right normalization for α, but the observation in Nicoud *et al.* (2001) that the effect of the control is mainly felt on the velocities near the wall suggests that h is not a relevant length scale, and that a more natural normalization would be wall units. The value recommended by Nicoud *et al.* (2001) is then $\alpha^+ \approx 6 \times 10^{-2}$, and results in $\sigma/\sigma_P \approx 2 \times 10^{-3}$. Both the small magnitude of the dimensionless α and of the ratio of the standard deviations strongly suggest that the system is overcontrolled.

A detailed analysis of the effect of α is beyond the scope of this work, and it was not attempted, but a simple approximation of the cost function can be used to estimate the relevant trends. Assume that the velocity u near the wall is essentially a (random) function of the local wall stresses, $u = f(\tau^w)$, where all the equations in the following

argument have to be understood as being applied at a given x and z. We can then approximate the cost function as,

$$\mathcal{J} \approx 2\delta(\overline{u} - U_{ref})^2 + 2\alpha\overline{(\tau^{w\prime})^2}, \tag{3.3}$$

where δ is a measure of the height over which the velocity is modified by the control, and u is taken at some representative distance from the wall of order δ. The factor of two reflects the contribution from both walls. The minimization of $\mathcal{J}$ requires that its derivative with respect to all the τ^w should vanish, giving for each grid point

$$\frac{\partial \mathcal{J}}{\partial \tau^w} = 4\delta \frac{\overline{u} - U_{ref}}{N_x N_z} \frac{df}{d\tau^w} + 4\alpha \frac{\tau^{w\prime}}{N_x N_z} = 0, \tag{3.4}$$

where we have assumed that $\overline{\tau^w}$ does not depend of the control. Assuming that $f(\tau^w)$ can be linearized around $\overline{\tau^w}$ and expressing $\overline{u}$ in terms of $f(\tau^w)$, we obtain after some algebra that

$$\tau^{w\prime} = [U_{ref} - \overline{f(\overline{\tau^w})}] \frac{\delta f_\tau/\alpha}{1 + \delta \overline{f_\tau^2}/\alpha}, \tag{3.5}$$

where f_τ is $\mathrm{d}f/\mathrm{d}\tau^w$ evaluated at $\overline{\tau^w}$. This is an interesting expression because it captures the tendency of τ'^w to increase with decreasing α, but saturates to some finite value when $\alpha \to 0$. In that limit the cost function becomes $\overline{u} - U_{ref} \propto \alpha$.

This has the simple interpretation that, if there is a solution to the unconstrained control problem, i.e. if there is a τ^w such that the first term in (2.1) vanishes, the control algorithm approximately identifies it for some small value of α, and any further decrease in α does not change that solution appreciably. If such solution does not exist, τ'^w and u' would diverge as α^{-1} when $\alpha \to 0$, and the cost function would saturate to some non-zero minimum value. This would appear in our simple model as $\overline{f_\tau^2} = 0$.

We tested this behavior by running case **S2**, in which α was divided by four with respect to the two other cases. The new value of α decreases σ/σ_P, as expected, while the mean velocity profile improves everywhere (figure 2*a*), and the intensity of the velocity fluctuations near the wall increases (figure 2*b*). All this is in qualitative agreement with the previous analysis. The ratio between the standard deviations of the wall stresses in cases **S2** and **S1** is 2:1, which is smaller than the ratio of 4:1 which would correspond to an α^{-1} behavior, and suggests some degree of saturation towards an exact solution.

To test whether such a solution exists, a second experiment was run with $\alpha = 0$. The velocity fluctuations grew still further, apparently without bound, leading to numerical instability for any given constant time step. When the code was modified to run at a constant CFL, we were able to trace the growth of the fluctuating velocities in the first plane off the wall to values of the order of $u'^+ \approx 600$, implying that the suboptimal boundary conditions, at least in their present form, are not able to drive the LES to full agreement with the desired profile. The errors in figure 2(*a*) suggest that the difficulty is not with the behavior of the near-wall region, but with the center of the channel. It is an interesting, although unresolved, question whether this is a limitation of the LES model itself, which cannot reproduce the phenomena responsible for the wake component, or of the boundary conditions.

3.2. *Rough walls*

The most important effect of roughness on the mean velocity above the buffer zone is a constant velocity decrement, ΔU^+ (Raupach *et al.* 1991; Jiménez, to appear 2004). A second effect is a shift Δy in the wall-normal coordinate, due to the uncertainty in

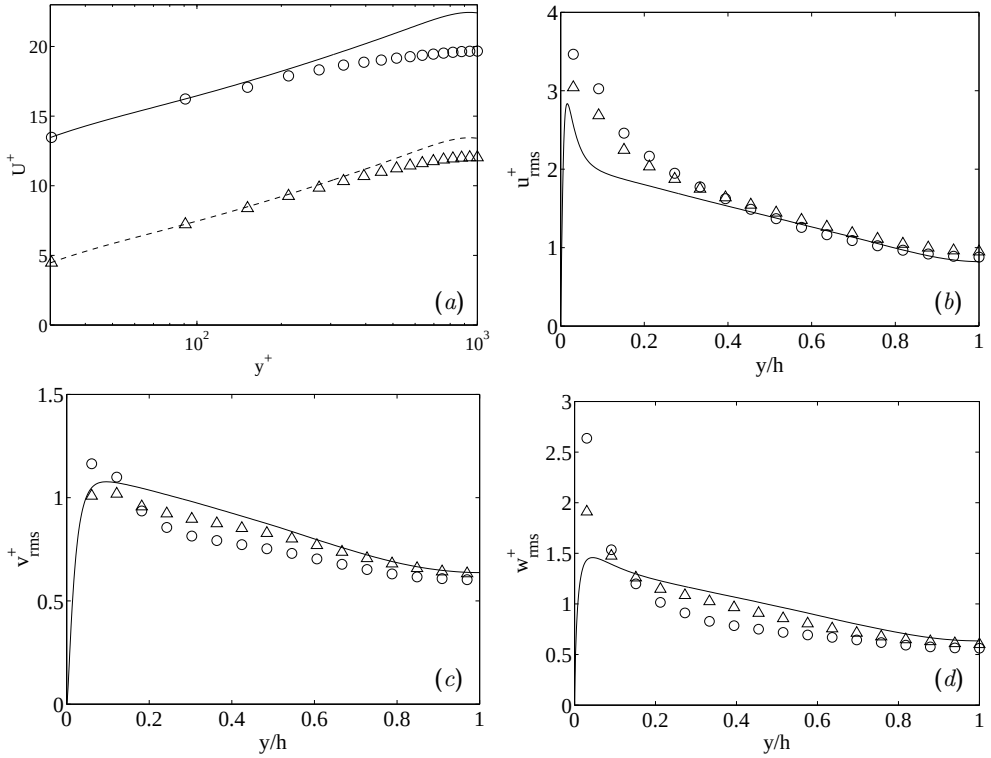

FIGURE 3. (*a*) Mean velocity profiles. (*b*) Streamwise velocity fluctuations. (*c*) Wall-normal velocity fluctuations. (*d*) Spanwise velocity fluctuations. ——— , smooth wall DNS, $Re_\tau = 950$; - - - - , reference velocity profile for the rough case; ○ , case **S1**; △ , case **R1**.

the position of the wall. In our case, in which the velocity is only computed at fairly large values of y^+, the wall-normal shift is negligible and the mean velocity profile can be written as

$$U^+(y^+) = \frac{1}{\kappa}\log(y^+) + 8.5 - \frac{1}{\kappa}\log(k_s^+) + \frac{1}{\kappa}\Pi(y/h), \tag{3.6}$$

or

$$U^+(y^+) = \frac{1}{\kappa}\log(y^+) + 5.1 - \Delta U^+ + \frac{1}{\kappa}\Pi(y/h), \tag{3.7}$$

were Π is the wake function, and either ΔU^+ or k_s^+ characterize the effect of roughness on the mean velocity profile.

Using equation (3.7) we construct our rough mean velocity profile for case **R1** just subtracting a constant $\Delta U^+ = 9^+$ from the smooth mean velocity profiles in del Álamo *et al.* (2003). This corresponds to a fully-rough flow with an equivalent sand roughness $k_s^+ \approx 140$.

3.3. *Statistics*

Figure 3 shows the mean velocity and the velocity fluctuations profiles for cases **S1** and **R1**. The mean velocities share some characteristics with those obtained by Nicoud *et al.* (2001), even though the latter used as reference profile a logarithmic law without a wake function. The error between the mean velocity and U_{ref} is given in figure 4 for the three cases computed. It is quite small near the wall, but grows to $O(1)$ at the

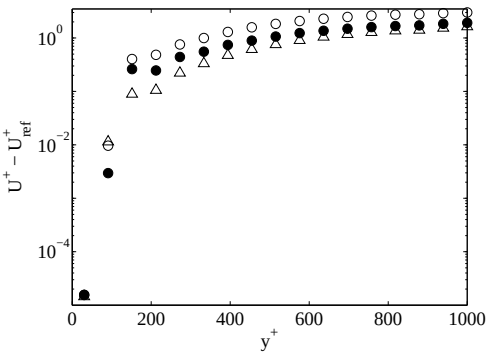

FIGURE 4. Error in the mean velocity profiles with respect to their references. ○ , case **S1**; ● , case **S2**; △ , case **R1**.

center of the channel. Between the second and the third grid point there is a weak discontinuity that changes the intercept of the logarithmic law. Its origin is probably the spatial discretization, because it appears at the same grid point in Nicoud *et al.* (2001) even if their resolution is coarser than ours by a factor of four.

The root-mean-squared velocity fluctuations are presented in figures 3(b), 3(c) and 3(d). The streamwise and spanwise fluctuations near the wall are higher in all the large-eddy simulations than in the direct simulation, although the agreement is quite good in the core region for the streamwise direction. The wall-normal and spanwise fluctuations are slightly underpredicted by the suboptimal code in the core region. The high values for the streamwise velocity fluctuations near the wall and the velocity fluctuations in the core region agree with the results of Nicoud *et al.* (2001), but the exceptionally high values of the spanwise velocity fluctuations near the wall shown in figure 3(d) do not.

The lower values of the velocity fluctuations near the wall in case **R1** with respect to **S1** are consistent with the effect of roughness on physical turbulence. This is often interpreted as the interference of the roughness elements with the smooth-wall self-sustaining turbulence cycle (Jiménez & Moin 1991), as explained by Jiménez (to appear in 2004). This interpretation is unlikely in the present case because the resolution is too coarse in all three directions to capture the scales associated with the regeneration cycle, and the most likely explanation is that the decrease of the fluctuations is due to the lower turbulence production near the wall due to the weaker velocity gradients across the first grid element of the rough reference profile.

The wall stresses τ^w_{xy} and τ^w_{zy} provided by the control algorithm are studied using their probability density functions (p.d.f.), which are shown in figure 5. They are compared at $y^+ = 60$ with the p.d.f.'s of the shear stresses in a DNS channel with $Re_\tau = 550$ (del Álamo *et al.* 2003), after box-averaging the latter to the LES grid ($\Delta_x \times \Delta_z = 196^+ \times 65^+$). Although it was not possible to post-process the shear stresses from the $Re_\tau = 950$ in time for this report, there is probably little differences between them an those at $Re_\tau = 550$, because this part of the flow scales approximately in wall units.

It is clear from figure 5(a) that the τ^w_{xy} in the suboptimal simulations are different from the DNS one, especially in that the former are not able to reproduce the asymmetry of the p.d.f. and try to reproduce the mean value of the shear stresses by displacing their modes to positive values. As expected, the standard deviations behave in the same way as the velocity fluctuations, **R1** < **S1** < **S2**. Figure 5(c) and 5(d) show the p.d.f.'s of the three cases when the stresses are normalized with theirs mean value $\langle\tau\rangle$ and standard

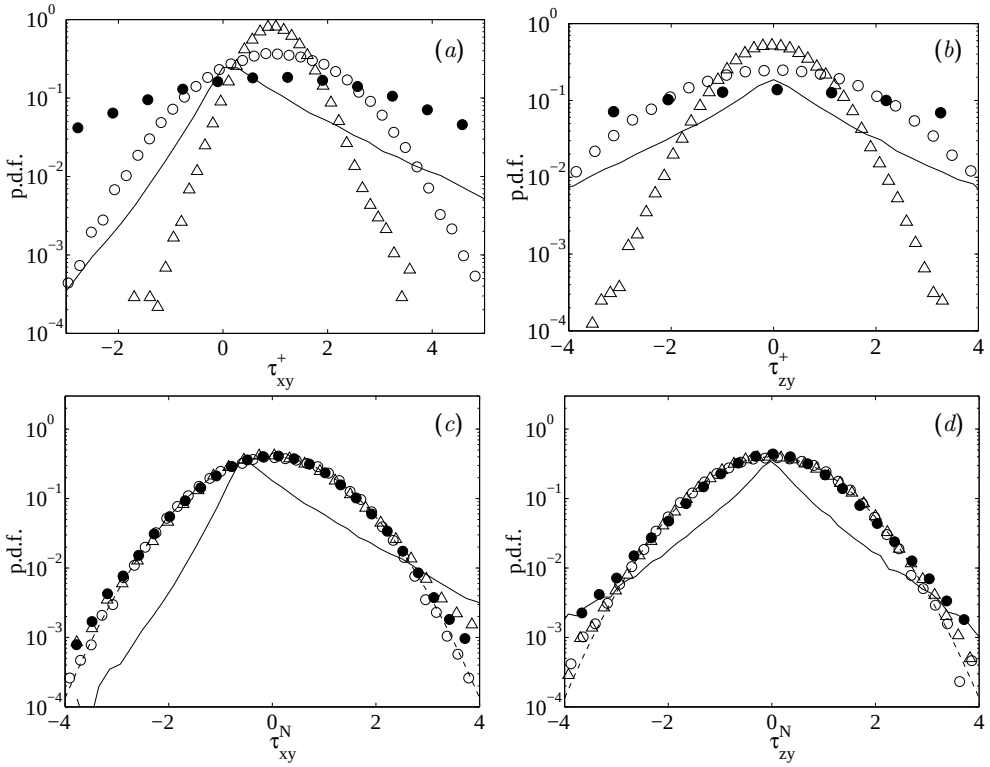

FIGURE 5. Probability density functions (p.d.f.) of the shear stresses at the wall. The shear stresses in figures (*a*) and (*b*) are expressed in wall units, while in figures (*c*) and (*d*) they are normalized as in equation (3.8). ——— , DNS (see text for details); - - - - , Gaussian; ○ , case **S1**; • , case **S2**; △ , case **R1**.

deviation σ_τ,

$$\tau^N = \frac{\tau - \langle\tau\rangle}{\sigma_\tau}. \tag{3.8}$$

The collapse of the three curves on the Gaussian distribution, and the differences with the DNS results, suggest that there is little physical information on the shear stresses given by the control algorithm.

Another way of characterizing the shear stresses given by the control is the study of their spectral distribution. We can define the spectrum E_{ij}

$$E_{ij}(k_x, k_z) = \langle\widehat{\tau}_{ij}\widehat{\tau}^*_{ij}\rangle, \tag{3.9}$$

where $\widehat{\tau}_{ij}(k_x, k_z)$ are the Fourier coefficients of the two-dimensional Fourier transform of the wall stresses τ^w_{ij}. The asterisk * indicates complex conjugation and k_x,k_z are the wave numbers.

Figure 6 shows these premultiplied spectra for the cases **S1** and **R1**, as functions of the wavelengths $\lambda_x = 2\pi/k_x$ and $\lambda_z = 2\pi/k_z$. Because each spectrum is normalized with its maximum, it only contains information about the wavelengths. There is very little differences between the two cases.

It is important to notice that the most energetic modes are located in the large-wavelength end of the spectra, specially as regards their widths. The 'infinitely wide'

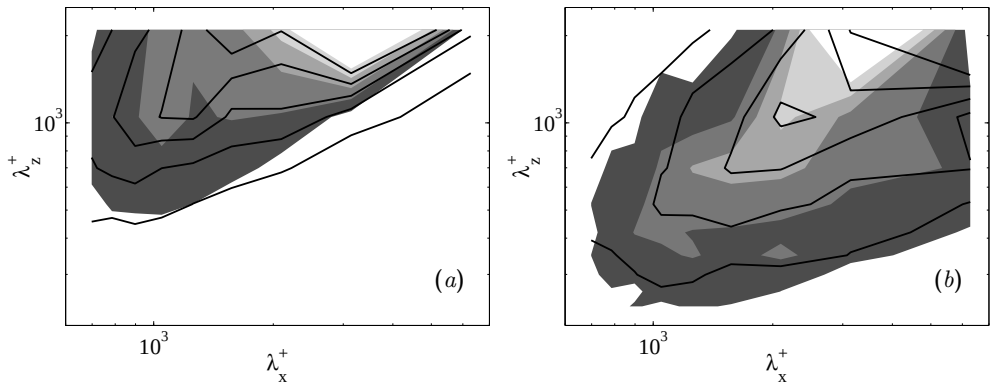

FIGURE 6. Two-dimensional premultiplied spectra of the stresses at the wall as functions of the streamwise and spanwise wavelengths. (a) E_{xy}, (b) E_{zy}. Shaded contours are from the **S1** case and lines are from **R1**. Each spectrum is normalized with its maximum.

$(\alpha, 0)$ modes for the τ_{xy}^w spectrum sums up to 26% of the energy in the smooth case and to 35% in the rough one, but the energy in the 'infinitely long' $(0, \beta)$ modes is below 1% of the total in both cases. On the other hand, for the τ_{zy}^w spectrum the energy contained in the $(\alpha, 0)$ modes is negligible, while the energy contained in the $(0, \beta)$ modes sums 7% of the total energy in the smooth case and 9% in the rough case. That suggests that the spectrum of τ_{xy}^w is wider, but not too much longer than the simulation box, while the τ_{zy}^w spectrum almost fits in it. The behavior of this quantity in the DNS is not known.

It is interesting to analyze how the control variable characteristics affect flow variables such as the velocities. In order to do that, we have studied the energy spectrum of the velocity components, E_{uu}, E_{vv} and E_{ww}, defined as

$$E_{uu}(k_x, k_z) = \langle \hat{u}_{kx,kz} \hat{u}^*_{kx,kz} \rangle_T \tag{3.10}$$

The corresponding one-dimensional spectra are obtained adding equation (3.10) over a certain direction in Fourier space.

Figures 7(a) and 7(b) show the one-dimensional premultiplied spectrum of the streamwise velocity components at $y^+ = 30$, which is the first grid point in the mesh. Although the gradient of this variable is determined directly by the control, the agreement between the suboptimal cases and the DNS results is reasonable good, at least as much as can be expected from the coarse grid being used. The same happens for the wall-normal velocity component (not shown here), but not for the spanwise component, whose spectrum is shown in figures 7(c) and 7(d). The spanwise velocity has a very energetic mode which spans the full width of the box and almost all of its length. When the instantaneous velocity fields are examined, we observe fairly regular diagonal bands of positive or negative spanwise velocity. This is reminiscent of the instabilities observed by Jiménez *et al.* (2001) in a channel with a porous wall, where they were traced to a coupling between a weakly-damped mode of the impermeable channel and the porous-wall condition. In that case the result was a series of spanwise rollers spanning the full height and width of the channel, and it is conceivable that a similar coupling might result in the present structures.

The spurious perturbation of the spanwise velocity disappears as we move a few grid points away from the wall, as can be observed in the spectra in figures 8. This relatively fast relaxation away from the wall of the defects of the wall layer, which recalls the similar

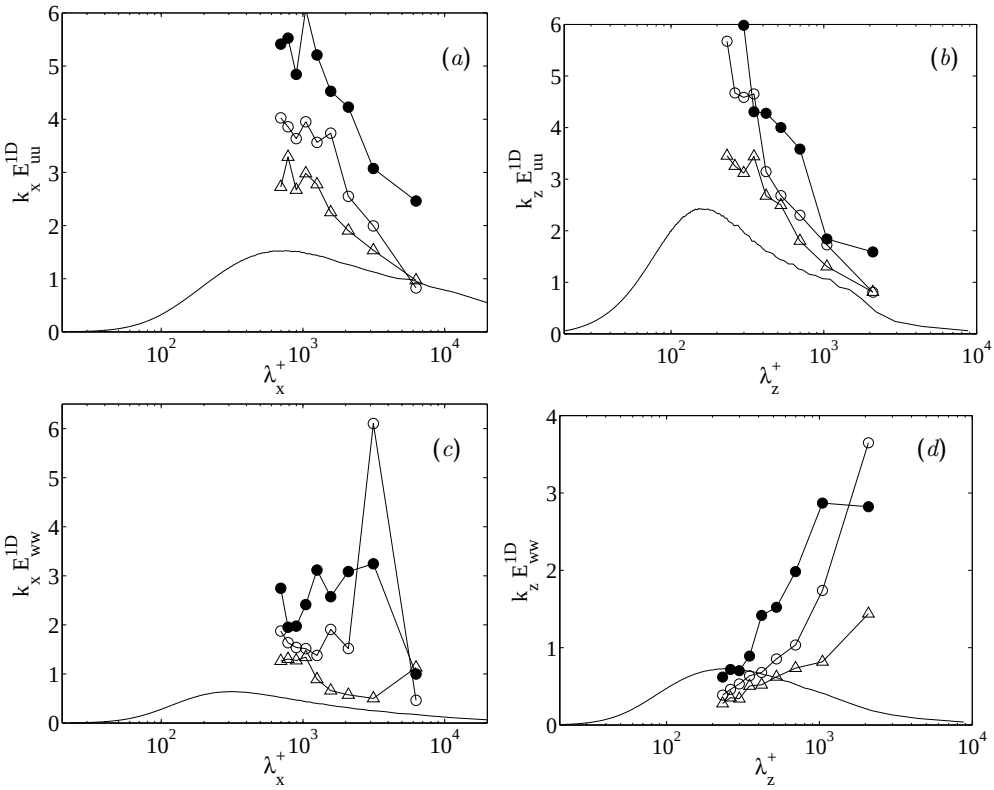

FIGURE 7. One-dimensional premultiplied velocities spectra at $y^+ = 30$, normalized in wall units and plotted as functions of the wavelengths λ_x (a, c) and λ_z (b, d). (a) and (b), streamwise component; (c) and (d) spanwise component. ——— , DNS; ○ , case **S1**; ● , case **S2**; △ , case **R1**.

relaxation of the fluctuation intensities in figures 2(b) and 3(b), suggests that the effect of the wall is relatively local to small values of y, and that the main role of the boundary conditions is to provide a correct intercept for the mean velocity.

4. Conclusions

In this work we have simulated three channel flows using the suboptimal-control code developed by Nicoud *et al.* (2001), after some modifications to improve its performance. We have seen that the suboptimal control code is not able to reproduce the wake component of the mean velocity profile of real channels. The magnitude of the error depends on the parameter α which weights the energy of the control in the cost function. Decreasing this parameter decreases the error in the wake, but degrades the agreement of the velocity fluctuation intensities near the wall. A simplified analysis of two numerical experiments with different values of α suggests that the problem with the velocity profile near the channel centerline is intrinsic to the simulation procedure, and not a consequence of the boundary condition algorithm. This result, together with the reorganization of the flow structures away from the wall, raises the question of whether it is possible to control the whole flow just by acting on the wall.

There are also open questions about the effects of α on the mean velocity profile and

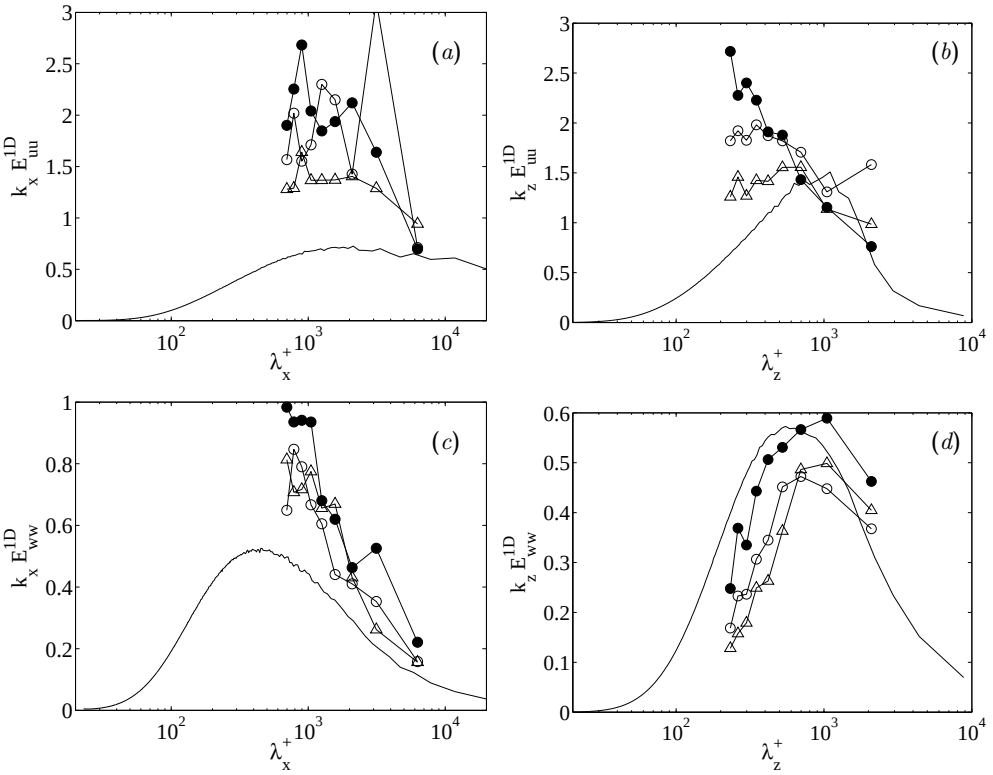

FIGURE 8. One-dimensional premultiplied velocities spectra at $y^+ = 150$, normalized in wall units and plotted as functions of the wavelengths λ_x (a, c) and λ_z (b, d). (a) and (b), streamwise component; (c) and (d) spanwise component. ——— , DNS; ○ , case **S1**; ● , case **S2**; △ , case **R1**.

on the root mean squared velocity fluctuations, where the influence of this parameter seems to be more important. More work is needed in that direction.

We have shown that the suboptimal code is able to match a synthetic profile for a rough turbulent channel, and that the trend of the changes in the root-mean-squared velocity fluctuation profiles agrees with the expected results. It is not clear whether this agreement is due to a change in the physics of the wall, or just a secondary effect of a lower mean velocity gradient. However, the information gathered from the spectra and from the p.d.f.'s point to the latter explanation, as there are no clear differences between the structures near the wall in the smooth and the rough cases, except for the intensities. The structure of the wall stresses introduced by the control algorithm bear little resemblance to the corresponding physical quantities.

There are in all the present simulations a spurious organization of the near-wall spanwise velocity into large diagonal modes, which is most likely due to some instability of the control procedure, but which also disappears a few grid points away from the wall. Its analysis also requires further work.

5. Acknowledgments

This work was supported in part by the Spanish Comisión Interministerial de Ciencia y Tecnología, under grant BFM2000-1468, and by the Center for Turbulence Research.

The computational resources provided by the Centro de Investigaciones Energiéticas, Medioambientales y Tecnológicas in Madrid are gratefully acknowledged. We thank Dr. Meng Wang for his careful reading of a first version of this manuscript.

REFERENCES

Del Álamo, J.C., Jiménez, J., Zandonade, P. & Moser, R.D. 2003 Scaling of the energy spectra of turbulent channels. Submitted *J. Fluid Mech.*

Jiménez, J. 2004 Turbulent Flows over Rough Walls. *Ann. Rev. Fluid Mech.* **36**

Jiménez, J. & Moin, P. 1991 The minimal flow unit in near wall turbulence. *J. Fluid Mech.* **225**, 221-240

Jiménez, J., Uhlmann, M., Pinelli, A. & Kawahara, G. 2001 Turbulent shear flow over active and passive porous surfaces. *J. Fluid Mech.* **442**, 89-117

Nicoud, F., Baggett J. S., Moin, P. & Cabot, W. 2001 Large eddy simulation wall-modeling based on suboptimal control theory and linear stochastic estimation. *Phys. fluids.* **13**, 2968-2984

Press, W. H., Flannery, B. P., Tukolsky, S. A. & Vetterling, W. T. 1993 *Numerical Recipes in FORTRAN 77: The Art of Scientific Computing.* Cambridge University Press.

Raupach M.R., Antonia R.A., & Rajagopalan S. 1991 Rough-wall turbulent boundary layers. *Appl. Mech. Rev.* **44**, 1-25